Chemical Engineering Journal 452 (2023) 139519

Contents lists available at ScienceDirect

Chemical Engineering Journal

journal homepage: www.elsevier.com/locate/cej

The role of copper crystallization and segregation toward enhanced methanol synthesis via CO_2 hydrogenation over $CuZrO_2$ catalysts: A combined experimental and computational study

Francielle C.F. Marcos [a], Raphael S. Alvim [a], Lili Lin [b], Luis E. Betancourt [b], Davi D. Petrolini [c], Sanjaya D. Senanayake [b], Rita M.B. Alves [a], José M. Assaf [d], Jose A. Rodriguez [b,*], Reinaldo Giudici [a,*], Elisabete M. Assaf [c,*]

[a] Universidade de São Paulo, Escola Politécnica, Department of Chemical Engineering, Av. Prof. Luciano Gualberto, t. 3, 380, São Paulo, São Paulo ZIP 05508-010, Brazil
[b] Chemistry Department, Brookhaven National Laboratory, Upton, NY ZIP 11973, United States
[c] Universidade de São Paulo, São Carlos Institute of Chemistry, Av. Trabalhador São-Carlense, 400, São Paulo, São Paulo ZIP 13560-970, Brazil
[d] Universidade Federal de São Carlos, Rod. W. Luiz, km 235, São Paulo, São Paulo ZIP 13565-905, Brazil

ARTICLE INFO

Keywords:
CO_2 hydrogenation
Methanol
Mechanism
Cu-ZrO_2 interaction
DFT

ABSTRACT

The role of copper crystallization in the enhanced methanol production via CO_2 hydrogenation over $CuZrO_2$ catalysts was explored along with a combination of experimental and computational studies. The catalysts were synthesized by a surfactant-assisted route followed by reflux in a one-pot method. Catalyst structure, bulk properties, surface reactivity, and reaction pathways were evaluated by XRD, BET, FRX, TPR, N_2O-TPD, CO_2-TPD, *in situ* DRIFTS, AP-XPS, and XRD. Calculations based on density functional theory (DFT) were performed to explore the formation of possible intermediates in a copper-driven conversion with surface models of the $CuZrO_2$ catalyst. The combination of experiments and DFT results revealed that the intermediate steps of the catalyzed reaction of CO_2 hydrogenation into methanol might depend on the incorporation of Cu in the zirconia sample. The catalyst containing only amorphous interfacial sites showed higher performance on CO_2-to-methanol hydrogenation compared to the catalysts containing high crystallinity of copper. The superior activity of the $10CuZrO_2$ catalyst is mainly ascribed to the cooperative effect between the highly dispersed copper nanoparticles and the basic sites.

1. Introduction

Methanol production from carbon dioxide (CO_2) hydrogenation using green hydrogen (H_2) and waste CO_2 has attracted significant attention [1,2]. When green hydrogen is available, the usage of carbon dioxide seized from power plants or industrial processes can be a smart key plan to achieve a carbon-neutral system addressing environmental impacts and producing important vital materials [3] on behalf of the chemical and petrochemical industries [4–6].

Several studies have been performed on Cu-based catalysts to obtain the best methanol activity from CO_2 hydrogenation [7]. According to the literature, CuO/ZrO_2 catalysts have shown superior methanol selectivity in the CO_2 hydrogenation reaction than a trade $CuO/ZnO/Al_2O_3$ catalyst. Additionally, the interface of Cu with ZrO_2 is the key active site of this reaction [8–10].

Research with model catalysts has shown that the Cu-ZrO_2 interface is much more active than the Cu surface for CO_2 activation and methanol production [10]. In recent works, DFT reckoning has shed light on the important electronic properties of Cu-ZrO_2 catalysts. Using models of clusters of Cu supported on ZrO_2 [11] and supported ZrO_2 by Cu, [12] the CO_2 conversion into methanol is carried out by different catalytic routes notwithstanding always being energetically favorable. Therefore, understanding the chemistry occurring on the surface of Cu-ZrO_2 catalysts from DFT calculations can provide a further accurate outlook on the reactional properties for the design and development of superior heterogeneous catalysts.

However, even though experimental and computational studies have been extensively accomplished, the several roles of ZrO_2 in the catalytic process are still under consideration since the crystal phase has a

* Corresponding authors.
E-mail addresses: rodrigez@bnl.gov (J.A. Rodriguez), rgiudici@usp.br (R. Giudici), eassaf@iqsc.usp.br (E.M. Assaf).

https://doi.org/10.1016/j.cej.2022.139519
Received 22 May 2022; Received in revised form 29 August 2022; Accepted 27 September 2022
Available online 3 October 2022

Nomenclature

Roman letters

SA_{Cu}	metallic surface area of copper [m^2/g]
D_{Cu}	Cu dispersion [%]
$S_{B.E.T}$	specific surface area [m^2/g]
GHSV	space velocity: gas hourly space velocities [mL gh^{-1} $^{-1}$]
XCO_2	CO_2 conversion [%]

significant effect on the CO_2 activation mechanism. Zirconia oxide has four kinds of polymorphism: tetragonal, cubic, monoclinic, and amorphous (or zirconium hydroxide) [8]. As reported by the literature, the amorphous zirconia (a-ZrO_2) shows superior performance than the crystalline tetragonal (t-ZrO_2) and monoclinic zirconia (m-ZrO_2) phases [4,13,14].

This finding motivated the described investigation on the CO_2 hydrogenation over copper and a-ZrO_2-based catalysts. Therefore, Cu-ZrO_2 catalysts have been prepared by the one-pot method with a higher specific surface area compared with other catalysts (in a similar composition), where zirconia is present in an amorphous phase for all catalysts. Thereafter, the role of copper crystallization was evaluated in connection with enhanced methanol synthesis by systematically increasing copper loading.

In this article, experimental and computational studies were combined to understand the role of copper crystallization and segregation toward enhanced methanol production via CO_2 hydrogenation over $CuZrO_2$ catalysts, correlating activity with the loading of copper and the interaction of Cu with amorphous ZrO_2 in catalysts synthesized by the surfactant-assisted co-precipitation method in one step.

DFT calculations were performed to determine the specific adsorption energies of the CO_2, H_2, methanol, and H_2O molecules on the ZrO_2(−111) surface, including the conversion and dissociation processes. For that, different ZrO_2 surfaces were modeled through a Cu-adatom and by Cu-doping to simulate the Cu influence in the $CuZrO_2$ catalysts. In these conditions, we obtained the preferential intermediates formed in the process of CO_2 conversion into methanol. Therefore, it was possible to figure out some important electronic properties of the $CuZrO_2$ catalysts influenced by different Cu compositions experimentally analyzed. In particular, the intermediate steps of the reaction of CO_2 hydrogenation into methanol may depend on the Cu crystallization grade in the catalyst, with low copper crystallization boosting the methanol production.

2. Experimental section

2.1. The catalyst preparation

A series of catalyst-containing different Cu content (10–45 wt%) on ZrO_2 was prepared with the surfactant-assisted route followed by the reflux method. First, an aqueous solution containing $Cu(NO_3)_2{\cdot}3H_2O$ (Alfa Aesar), $ZrO(NO_3)_2{\cdot}xH_2O$ (Acros Organics), and Pluronic P-123® (EO)20(PO)70(EO)20 block copolymer surfactant, 1 % molar, (Sigma-Aldrich) were made under rapid stirring during 24 h. A precipitate was formed by simultaneously adding an aqueous solution of Na_2CO_3 1 M (Synth) to an aqueous solution containing the metals precursors and surfactant. The mixture was kept under stirring at a constant pH (~7) during the co-precipitation. The slurry formed was refluxed at 110 °C for 24 h. All solids had been filtered and washed with deionized water until pH 7. Afterward, the as-prepared precursors have been dried and calcined in air at 450 °C for 2 h with a heating rate of 5 °C min^{-1}. The materials were labeled as 10$CuZrO_2$, 20$CuZrO_2$, 30$CuZrO_2$, and 45$CuZrO_2$, where the numbers express the loading of copper in wt%.

2.2. Characterization of samples

X-ray powder diffraction patterns were performed on a Rigaku Multiflex diffractometer using Cu Kα (1.5406 Å) radiation source and 2θ = 10° to 80° at a 10° min^{-1} rate.

In situ time-resolved X-ray diffraction (XRD) measurement was carried out at the 17BM beamline of the Advanced Photo Source (APS) at Argonne National Laboratory (ANL), with an X-ray wavelength of 0.24172 Å. The XRD measurements under CO_2 hydrogenation reaction conditions (H_2/CO_2 3:1) have been performed at 250 °C for 20 min; a detailed course of action is written elsewhere [15].

N_2 adsorption/desorption measurements were performed in Micromeritics equipment, model ASAP 2020, at −196 °C. Firstly, the samples were outgassed under vacuum for 12 h at 250 °C; the detailed procedure is described in a recent study by our group[16]. The temperature-programmed reduction (TPR) analysis was carried out in Micromeritics Pulse ChemiSorb 2750 equipment; the specified methodology has been detailed by Marcos et al. [16].

The high-resolution transmission electron microscopy (HR-TEM) images were collected using a JEOL JEM 2100F instrument at the Center for Functional Nanomaterials at Brookhaven National Laboratory; detailed procedures are described elsewhere [15].

The temperature-programmed desorption (CO_2-TPD) and H_2-TPD experiments were conducted with the same equipment used for the TPR analysis. The CO_2-TPD analysis was described in detail elsewhere [16]. For H_2-TPD analysis, the material was activated with an 10 %H_2/Ar flow of 30 mL min^{-1} at 250 °C for 1 h and atmospheric pressure. After the activation process, the sample was cooled to 45 °C and further saturated in pure H_2 for 30 min, followed by flushing in Ar for 1 h. The H_2-TPD measurements were conducted in an Ar stream (25 mL min^{-1}) from room temperature to 500 °C at a heating rate of 5 °C min^{-1}. A thermal conductivity detector monitored the change of hydrogen signal.

The metallic copper surface area and the copper dispersion have been evaluated with the same equipment as the TPR analysis. The copper metallic surface area (SA_{Cu}) and Cu^0 dispersion (D_{Cu}) were determined using the method shown in the Supporting Information, Equations (1 and 2); a detailed procedure has been previously described elsewhere [16].

Ambient-pressure X-ray photoelectron spectroscopy data were collected in a commercial SPECS AP-XPS chamber equipped with a PHOIBOS 150 EP MCD-9 analyzer and Mg-Kα X-ray source at the Chemistry Division of Brookhaven National Laboratory (BNL) using. Detailed experiments are reported elsewhere [16,17].

In situ DRIFTS spectra have been acquired by an FTIR spectrometer (Bruker XSA) equipped with a Harrick cell and an MCT detector at the Chemistry Division of BNL. The spectra were expressed in units of Kubelka-Munk (K-M). 10 mg of catalyst was added into the Harrick cell with inner quartz wool filling at the bottommost of the cell. The sample was reduced in a mixture of H_2 and He (H_2: He 1:1 M ratio) under a flow rate of 20 mL min^{-1} at the copper reduction temperature for 1 h. Then, the experiments were carried out at 250 °C temperatures. The background spectrum (256 scans) with a resolution of 4 cm^{-1} was acquired at the same conditions as the reaction in He (2 mL min^{-1}) and H_2 (6 mL min^{-1}) flow.

2.3. The catalytic evaluation

The catalytic tests for methanol production from CO_2 hydrogenation were performed in a high-pressure Micro activity Effi reactor (PID Eng &Tech) containing 200 mg of catalyst diluted with 100 mg of silicon carbide (SiC). Before the reaction, the materials were activated with an H_2 flow of 30 mL min^{-1} at 250 °C for 1 h and atmospheric pressure. After the activation process, the experiments have been performed at temperatures ranging from 200 to 300 °C. For each experiment, the temperature was held over 2 h. The flow rates of pure H_2 and pure CO_2 were set at 30 mL min^{-1} and 10 mL min^{-1}, respectively, with a GHSV =

12,000 mL $g^{-1}h^{-1}$, and 30 bar of pressure. Effluent products were analyzed with online gas chromatographer (Agilent 7890B) equipped with a thermal conductivity detector (TCD), a flame ionization detector (FID), and three columns: DB-624, HP-Plot-Q, and HP Molesieve. CO_2 conversion was denoted as $X(CO_2)$, methanol selectivity as S(MeOH), and methanol formation rate as CH_3OH formation rate. CH_4 concentration in the outlet gas was lower than 1 %. Then, the carbon balance was estimated from the CO_2, CO, and methanol concentrations using the normalization method, carbon balance >99 %. Marcos et al. reported the schematic of the experimental setup and how the data have been calculated in detail [18]. The thermodynamic properties have been calculated using the Peng- Robinson (PR) equation of state by the iiSE (Industrial Integrated Simulation Environment) process simulator (IISE Ltd. – iiSE chemical process simulator company). The calculation has been performed similarly to Stangeland et al. [19].

2.4. DFT calculations

The calculations have been performed using the Density Functional Theory (DFT) as implemented in the Quantum ESPRESSO (QE) package [20–22]. For describing more accurately the long-range interactions in processes of surface interactions, the modern functional vdW-DF3-opt1 was used to treat exchange-correlation (XC) interactions [23]. Spin-polarized solutions of the Kohn-Sham equations and Gaussian smearing broadening for a Fermi-level smearing width with a value of 0.02 eV were employed. The adsorption energies have been calculated with the sum of the total energies of the products minus the reactants. More calculation features are in the Supporting Information.

The monoclinic phase of the ZrO_2 bulk was used to represent one possible structure of the ZrO_2 catalyst. The ZrO_2 surface in the [−111] direction along the *c*-axis was obtained cleaving the bulk. A vacuum layer of 15 Å was then used to generate the surface. From it, a supercell of dimensions (2×2) was built, having two main types of Zr sites: six- and seven-coordinated respectively with the rates of 0.75 and 0.25, in addition to the three-coordinated oxygen sites. Figures and more details are presented in the Supporting Information.

As the experimental results of *in situ* characterization under reaction conditions display the $CuZrO_2$ catalyst with Cu sites with oxidation states zero (Cu^0) and 1+ (Cu^{1+}), two ZrO_2 surfaces were modeled: one with Cu-adatom and the other with Cu-doping to represent the Cu^0 and Cu^{1+} sites, respectively. On the Cu-doping surface, two Zr atoms were replaced by two Cu atoms, and three surface oxygen vacancies have gotten generated to create the Cu^{1+} sites, maintaining the neutrality of the system. In addition to the perfect surface, two possible structures for the Cu-adatom and Cu-doping surfaces have been simulated. For more details about selected surfaces and their electronic properties see the Supporting Information.

According to the most stable theoretical models of the perfect ZrO_2 surface and with Cu-adatom and Cu-doping, the calculations of energy variation of the global reaction (**R**) of hydrogenation of CO_2 into methanol [24] were proposed to form the most probable intermediates through the ZrO_2 catalyst as follows:

$$CO_2 + 3H_2 \rightarrow H_3COH + H_2O \quad \text{(R)}$$

$$CO_2 + 3H_2 + 2ZrO_2 \rightarrow CO_2@ZrO_2 + 3H_2@ZrO_2 \quad \text{(R1)}$$

$$CO_2@ZrO_2 + 3H_2@ZrO_2 \rightarrow H_3COH@ZrO_2 + H_2O@ZrO_2 \quad \text{(R2)}$$

$$H_3COH@ZrO_2 + H_2O@ZrO_2 \rightarrow H_3COH + H_2O + 2ZrO_2 \quad \text{(R3)}$$

where **R1**, **R2,** and ***R3*** are the elementary steps of adsorption, conversion, and desorption, respectively. From the intermediate of **R2**, it was also possible to compute the dissociated intermediate. This occurs throughout the dissociation of the H_3COH and H_2O molecules on the ZrO_2 surfaces. Then, the possible dissociation reaction (R4) was calculated as follows:

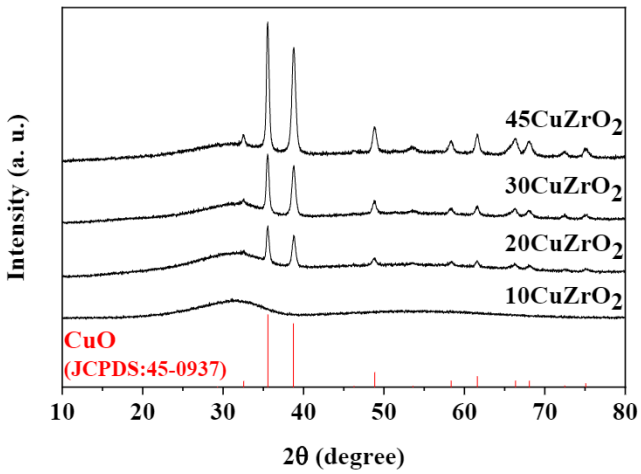

Fig. 1. XRD patterns of $CuZrO_2$ catalysts.

$$H_3COH@ZrO_2 + H_2O@ZrO_2 \rightarrow H_3CO^-H^+@ZrO_2 + OH^-H^+@ZrO_2 \quad \text{(R4)}$$

The specific step of reduction of CO_2 may be related to different processes, such as the H_2 dissociation. However, the H_2 adsorption tends to be more stable than the H_2 dissociation from ionic processes on oxide surfaces [25].

3. Results and discussion

3.1. Characterization of catalysts

The crystallinity of the samples had been initially evaluated by ex-situ XRD at room temperature, as shown in Fig. 1. The used synthesis method did not favor the crystallization of the copper and zirconia oxides in the sample with 10 wt% of copper or highly dispersed Cu particles below the detection limit of the technique were produced [8,25]. However, with an increase in Cu loading, from 20 to 45 wt%, CuO crystallization increased. The diffraction patterns at 2θ = 32.5°, 35.6°, 38.8°, 48.8°, 53.6°, 58.4°, 61.6°, 66.5° 68.1°, 72.3°, and 74.9° are assigned to CuO and matching to the monoclinic phase (JCPDS N° 45-0937) [26]. In all samples a broad halo peak of *ca.* 33° coinciding with ZrO_2 is observed, pointing to an amorphous or disordered at long-range zirconia [8], suggesting that the evaluated synthesis method did not favor the crystallization of ZrO_2. The ZrO_2 crystallization behavior agrees with the previous study [16], in which it was used the same surfactant and the one-pot method of synthesis.

Fig. S1 in the Supporting Information displays that the $CuZrO_2$ catalysts presented colors from light to darker green. As stated by the literature, the pale green for copper and zirconia powder catalysts consists of $Cu_aZr_{1-a}O_b$, where the copper could be incorporated into amorphous zirconia [8,9]. The dark green colors can indicate that there are both $Cu_aZr_{1-a}O_b$ and copper nanoparticles, due to the solubility limit of Cu species in amorphous zirconia. These observations agree with XRD (Fig. 1), where the sample with light green is amorphous, and with the increase in copper loading, the materials are dark colors, and the copper is crystalline also present.

Fig. S2 in Supporting Information shows the N_2 adsorption/desorption isotherms and the corresponding pore size distributions of $CuZrO_2$ catalysts. According to IUPAC, the samples displayed isotherms typical of mesoporous materials classified as type IVb with an H_2-type hysteresis loop. As can be seen in Fig. S2B, the increase of Cu loading from 10 to 30 wt% did not significantly alter the pore shape. However, with the copper increase to 45 wt%, the pore distribution has been broadened and the peak center has shifted to a larger pore size presumably due to the collapse of some pores in the course of the synthesis with the high copper loading.

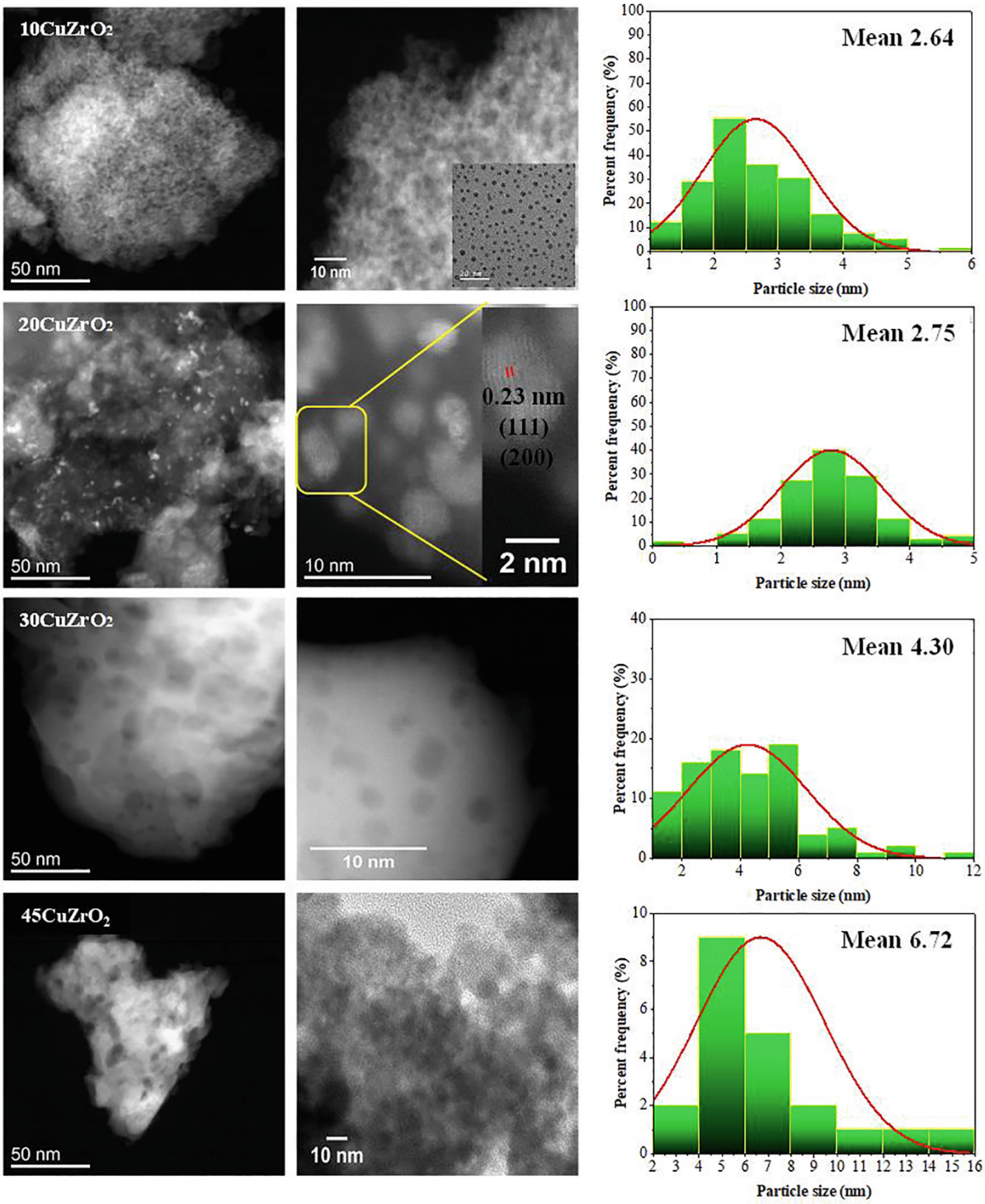

Fig. 2. Representative HRTEM images and subsequent metal particle size histograms of $CuZrO_2$ catalysts.

Fig. 2 depicts the metal particle size histograms of the $CuZrO_2$ catalysts corresponding to the HRTEM images. The increase in copper loading resulted in a higher copper particle size, which is composed of particles with an average crystallite size of 2–6 nm. Besides, one surface terminating plane attributed to (111) and (200) has been observed with respective interplanar spacings of 0.23 nm in the HRTEM image for the $20CuZrO_2$ catalyst, which is consistent with the crystalline plane of CuO [27]. It is difficult to distinguish between planes (111) and (200) because the lattice fringes are close, 0.2323 and 0.2310 nm, respectively.

To assess the reduction behavior of the $CuZrO_2$ catalysts H_2-TPR measurements were conducted, and the profiles are presented in Fig. S3A in Supporting Information. Peaks of reduction were observed, which is a characteristic of Cu^{2+} reduction to metallic copper ($CuO + H_2 \rightarrow H_2O + Cu^0$). There is a strong relationship between copper loading and H_2 consumption, with the increase in Cu loading the H_2 consumption raised. The literature review shows that ZrO_2 reduction does not occur in the evaluated temperature range (from 50 to 300 °C) [16]. Additionally, it was noted a shift in the onset of the reduction peak to higher temperatures with the increase in copper loading. According to

Table 1
Average mass percentage (wt.%) of Cu, specific surface area ($S_{B.E.T}$), total number of basic sites and (%) β peak, specific copper metallic area (SA_{Cu}), and copper dispersion (D_{Cu}) of catalysts.

Samples	Cu (%)	$S_{B.E.T}$ (m^2g^{-1})	Basic sites		D_{Cu} (%)[b]	SA_{Cu} (m^2/g_{Cu})[b]
			(mmol/g)[a]	β (%)		
ZrO_2	–	346	0.070	70.0	–	–
$10CuZrO_2$	10.0	441	0.048	73.3	8.0	15.3
$20CuZrO_2$	21.1	390	0.056	61.0	3.8	7.1
$30CuZrO_2$	29.2	285	0.047	64.0	3.5	6.7
$45CuZrO_2$	45.3	265	0.062	57.0	1.78	3.5

[a] determined by TPD-CO_2; [b] determined by N_2O chemisorption.

Table 2
The amount of H_2 desorption over $10CuZrO_2$ and $30CuZrO_2$ catalysts.

Samples	T (°C)	mmol/gcat	T (°C)	mmol/gcat
$10CuZrO_2$	25–280	0.73	280–500	1.41
$30CuZrO_2$		0.60		1.75

the literature [16], smaller particles of copper are reduced at lower temperatures, consistent with the data obtained from HRTEM analysis (Fig. 2).

The main physical-chemical properties of these catalysts can be compared from the data in Table 1. An increase in the Cu amount decreased the specific surface area. This might be owing to the formation of CuO crystalline at higher Cu loadings, as observed by XRD, which could block the pores of ZrO_2. Fig. S3B in the Supporting Information displays the CO_2 desorption profiles of the catalysts. These profiles are similar for all samples, with the first and highest CO_2 desorption peak from 50 °C to 125 °C and another from 125 to 300 °C, except for the catalyst with the lower copper loading. The peaks can be associated with weak and medium basic sites, respectively. The weakly basic sites (denoted as peak α) can be associated with hydroxyl groups (OH^-), while the moderate (denoted as peak β) can be associated with to metal-oxygen pair (Zr-O) [26,28,29] To understand the effect of these sites on the catalytic test, the peaks were integrated, and the results are also depicted in Table 1. According to the literature, the β peak is essential to promote CO_2 activation, resulting in the enhancement of methanol yield [29]. The samples presented the subsequent order of moderate (β) basic sites (%): $10CuZrO_2$ > $30CuZrO_2$ > $20CuZrO_2$ > $45CuZrO_2$. This difference in the basic sites could be correlated with the crystallization phase of copper, as presented by XRD patterns in Fig. 1, which can adsorb the CO_2 differently or due to the presence of oxygen vacancy in ZrO_2 that can act as active sites for CO_2 adsorption, as evidenced by Wang et al. [30]. Copper dispersion and metallic surface area followed the same behavior as the specific surface area ($S_{B.E.T}$), with the highest specific surface area showing the highest dispersion and copper surface area. It is deserving of pointing out that zirconia synthesized in this work presents a higher specific surface area than the materials found in the literature [31–35]. This confirms that the existence of a non-ionic surfactant in the synthesis of the materials influences the specific surface area.

Fig. S3C) shows the H_2 desorption profiles obtained for the pre-reduced $10CuZrO_2$ and $30CuZrO_2$ catalysts. Two H_2 desorption peaks were detected for both catalysts and labeled as α and β. The low

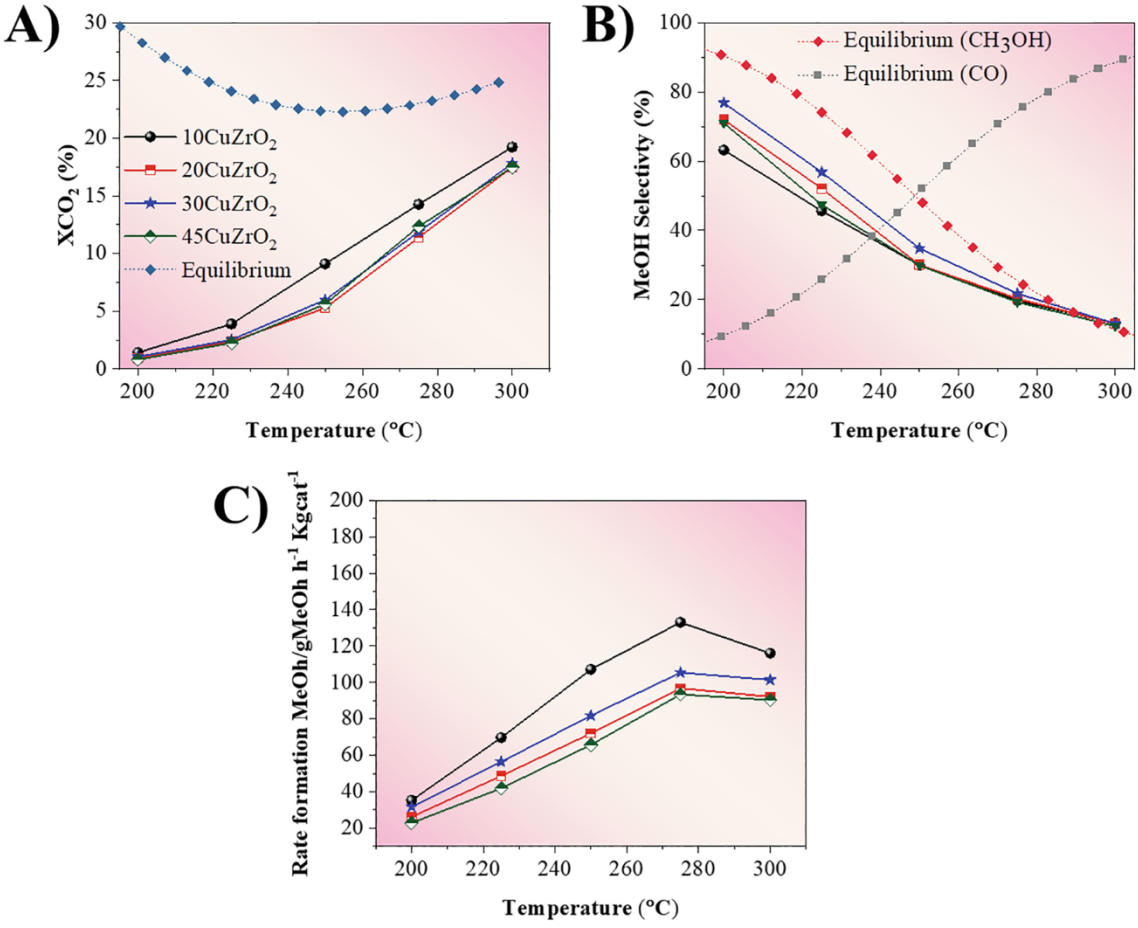

Fig. 3. A) CO_2 conversion B) Methanol selectivity, and C) methanol formation rate as a function of temperature over $CuZrO_2$ catalysts (GHSV = 12,000 mL $g^{-1}h^{-1}$), and the chemical equilibrium was predicted by gas-phase thermodynamics.

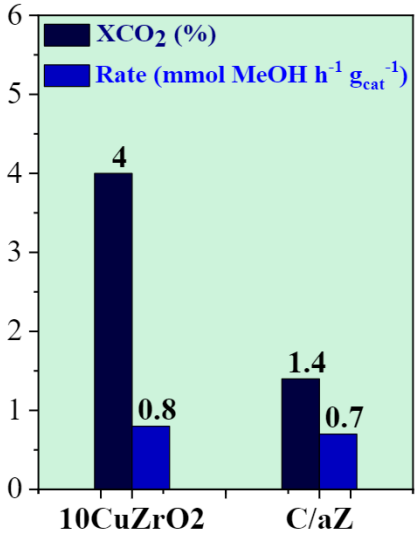

Fig. 4. Catalytic performance comparison of $10CuZrO_2$ and C/aZ [9] catalysts. Reaction conditions: W/Ftotal = 430 mg_{cat} s mL(STP) $^{-1}$, $CO_2/H_2/N_2$ = 1/3/1, 500 mg of catalyst at 230 °C and 10 bar.

temperature broadened peak (α) corresponds to the desorption of the chemisorbed hydrogen on the highly dispersed copper nanoparticles, which is related to the number of active sites for dissociation of hydrogen molecule to hydrogen atoms and the hydrogen atom on the surface of metal oxides caused by the spillover of hydrogen from the copper surface, while the higher temperature (β) centered at about 400 °C represents desorption of strongly adsorbed hydrogen over bulk CuO and ZrO_2 surface [36–38]. The increase of copper loading shifts the α peak toward higher temperature indicating a higher adsorption strength of the H atom on the surface of metal oxides. Table 2 presents the quantitative data of H_2 desorptions over both catalysts as a function of the temperature. The increase of Cu loading has not boosted the amount of H_2 adsorbed at low temperatures (α). The catalyst with lower copper content, $10CuZrO_2$, showed a higher amount of the α peak when compared to the $30CuZrO_2$ catalyst. This result is in line with the metallic copper area (Table 1). As reported by the literature, only the H_2 desorbed at lower temperatures is useful for synthesizing methanol from CO_2 hydrogenation [36–38].

3.2. Catalytic results

The performance of the $CuZrO_2$ catalysts with different copper loading was assessed in the methanol production by CO_2 hydrogenation as a function of the temperature at 30 bar until reaching the steady-state and under kinetic conditions (far away from the equilibrium conversion) to approach the intrinsic activity. Fig. 3 shows that the increase in temperature favored the CO_2 conversion for all catalysts. The catalyst with the lower amount of copper ($10CuZO_2$) leveraged the best CO_2 conversion. It is important to emphasize that this catalyst showed the highest values of copper dispersion, % medium basic sites, higher H_2 desorbed at lower temperature, metallic area, and the lower copper particle size, as presented in Table 1. Also, this catalyst has an amorphous structure for both phases (CuO and ZrO_2) or CuO is highly dispersed. Therefore, these properties favored the catalytic activity of this catalyst when compared with the catalysts with the crystalline structure of copper.

The products obtained were methanol, CO, and methane (less than 1 % of selectivity). The best methanol selectivity has been reached at 200 °C (Fig. 3B) by the $30CuZrO_2$ catalyst, which has a crystalline copper phase. The increase in the temperature from 225 °C to 300 °C decreased the selectivity of methanol but favored the reverse of the water-gas shift reaction (RWGS: $CO_2 + H_2 \rightarrow CO + H_2O$). The increase in copper loading did not boost the methanol selectivity at higher temperatures. The lower activity for the catalyst with the highest copper loading, $45CuZrO_2$, could be explained by the lower CO_2 adsorption and copper metallic area, as shown in Table 1. At high temperatures, 300 °C, both the amount of copper and the copper crystalline phase did not leverage the methanol selectivity. Alternatively, as displayed in Fig. 3C, the methanol formation rate was influenced by these variables. The methanol formation rate increased with the temperature to 275 °C. The lower methanol production at lower temperatures could be explained due to the high thermodynamic stability of CO_2 that requires high temperature for its conversion, which means that fewer molecules are produced, and due to RWGS reaction that occurs at the same temperature.

The activity presented by the ZrO_2 support has been negligible in this study, at 250 °C and 30 bar, with a low XCO_2 (0.18 %). The major selectivity was reached CO (82.8 %) with lower selectivity for MeOH and CH_4 (11.6 % and 5.6 %, respectively).

To compare the data of this research with a promising catalyst in CO_2-to-methanol hydrogenation, C/aZ [9], from the literature, a new experiment has been performed under the same reaction conditions, Fig. 4. It is important to highlight that the C/aZ catalyst has similar

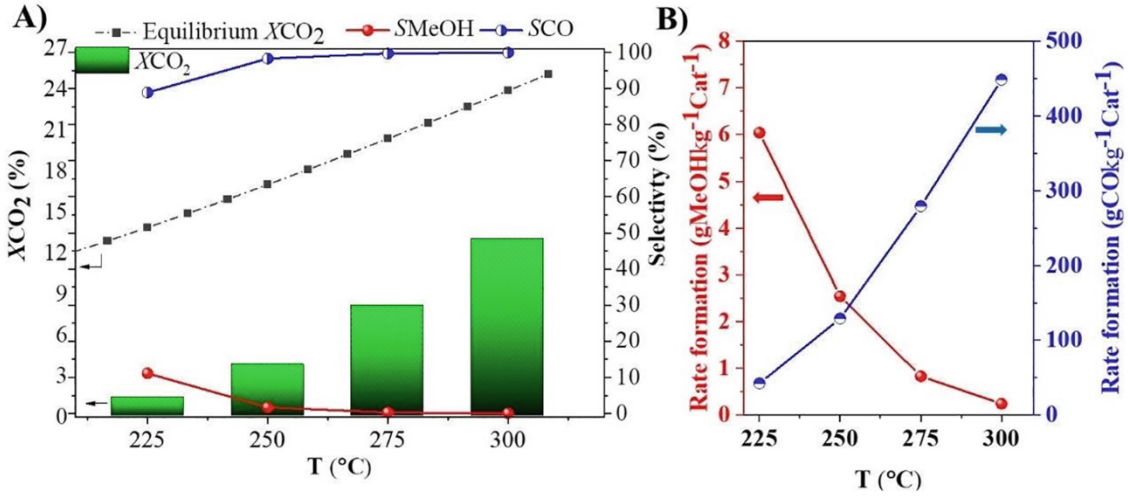

Fig. 5. A) CO_2 conversion and product selectivity as a function of the temperature of $30CuZrO_2$ catalyst and B) Effect of temperature on methanol and CO rate formation. Conditions: at 1 bar and GHSV = 123.1 mL min^{-1} g^{-1}.

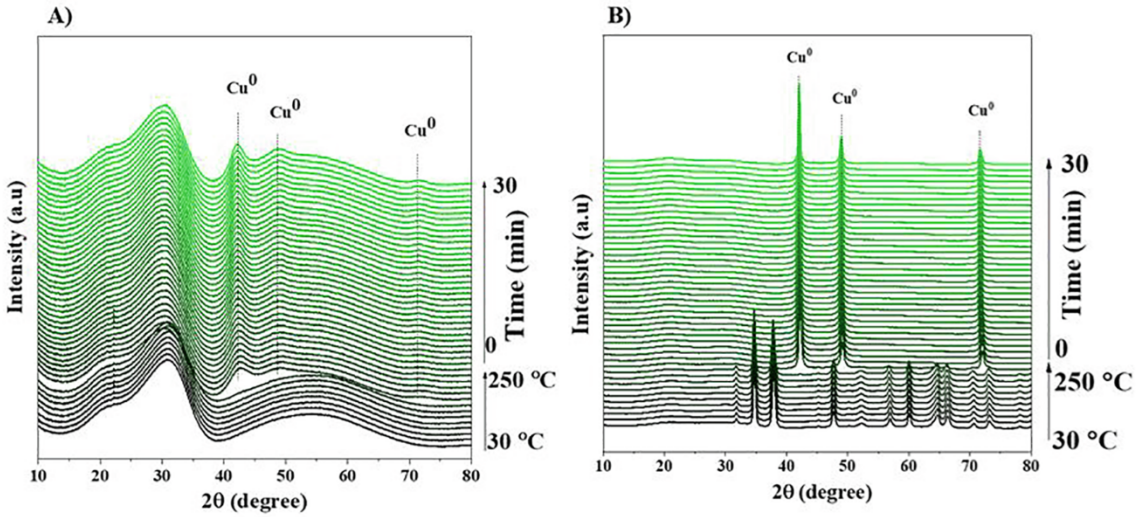

Fig. 6. *In situ* time-resolved XRD patterns of catalysts under activation conditions from 30 °C to 250 °C at 10 °C min^{-1} and during 30 min at 250 °C, 50 %H_2/He (6 mL min^{-1}): A) 10$CuZrO_2$ and B) 30$CuZrO_2$.

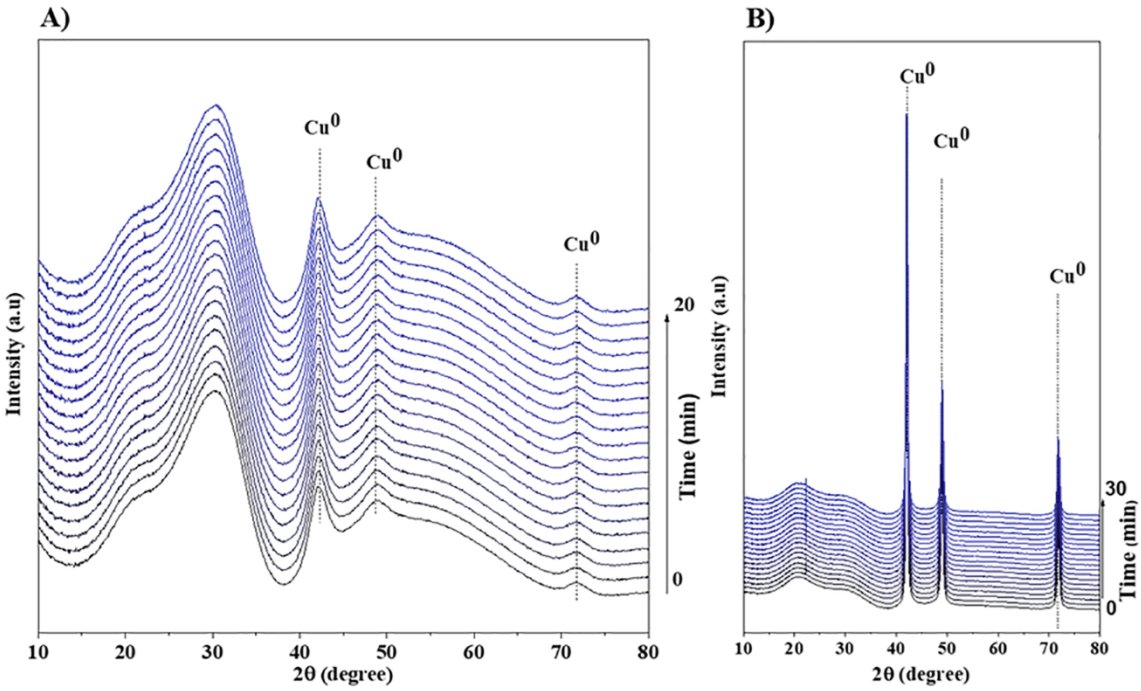

Fig. 7. *In situ* time-resolved XRD patterns of catalysts under reaction conditions at 250 °C, CO_2 (2 mL min^{-1}) and H_2 (6 mL min^{-1}): A) 10$CuZrO_2$ and B) 30$CuZrO_2$.

copper loading and both copper and zirconia phases in the amorphous state compared with the 10$CuZrO_2$ catalyst explored in this study. C/aZ catalyst showed at 10 bar XCO_2 <2 % and the methanol formation rate of 0.7 mmol MeOH h^{-1} g_{cat}^{-1} [9]. The 10$CuZrO_2$ catalyst reached an XCO_2 = 4 % with a methanol formation rate of 0.80 mmol MeOH h^{-1} g_{cat}^{-1}. Thus, it can be assumed that the merge of both amorphous ZrO_2 and Cu with a suitable copper loading is a promising catalyst in CO_2-to-methanol hydrogenation. The superior activity of the 10$CuZrO_2$ catalyst is due to the synthesis method that provided a higher specific surface area as shown by B.E.T analysis and different physical chemistry properties that may have favored the CO_2 adsorption/desorption to produce methanol.

To gain insight into the behavior at a system with lower pressure (1 bar) on the catalyst that reached the best methanol selectivity at low temperature, 30$CuZrO_2$, and correlate the results with physicochemical characterizations that were obtained *in situ,* under the same conditions, additional experiments have been made. As shown in Fig. 5A, the catalyst exhibited high CO_2 conversion at 300 °C. At 225 and 250 °C, the CO_2 conversion is below 5 %. As the temperature increases to 275 and 300 °C, CO_2 conversion increases, and the products were the same, mainly CO and low amounts of methanol and methane, although the catalytic activity is limited by the equilibrium [39]. As expected, at this low-pressure regime, regardless of the temperature of the reaction, a higher rate of CO is observed likened to the rate of methanol produced (Fig. 5B). This explains the reasons why methanol production is favored at high pressures, and it is typically carried out at 250 °C and 20 bar [40].

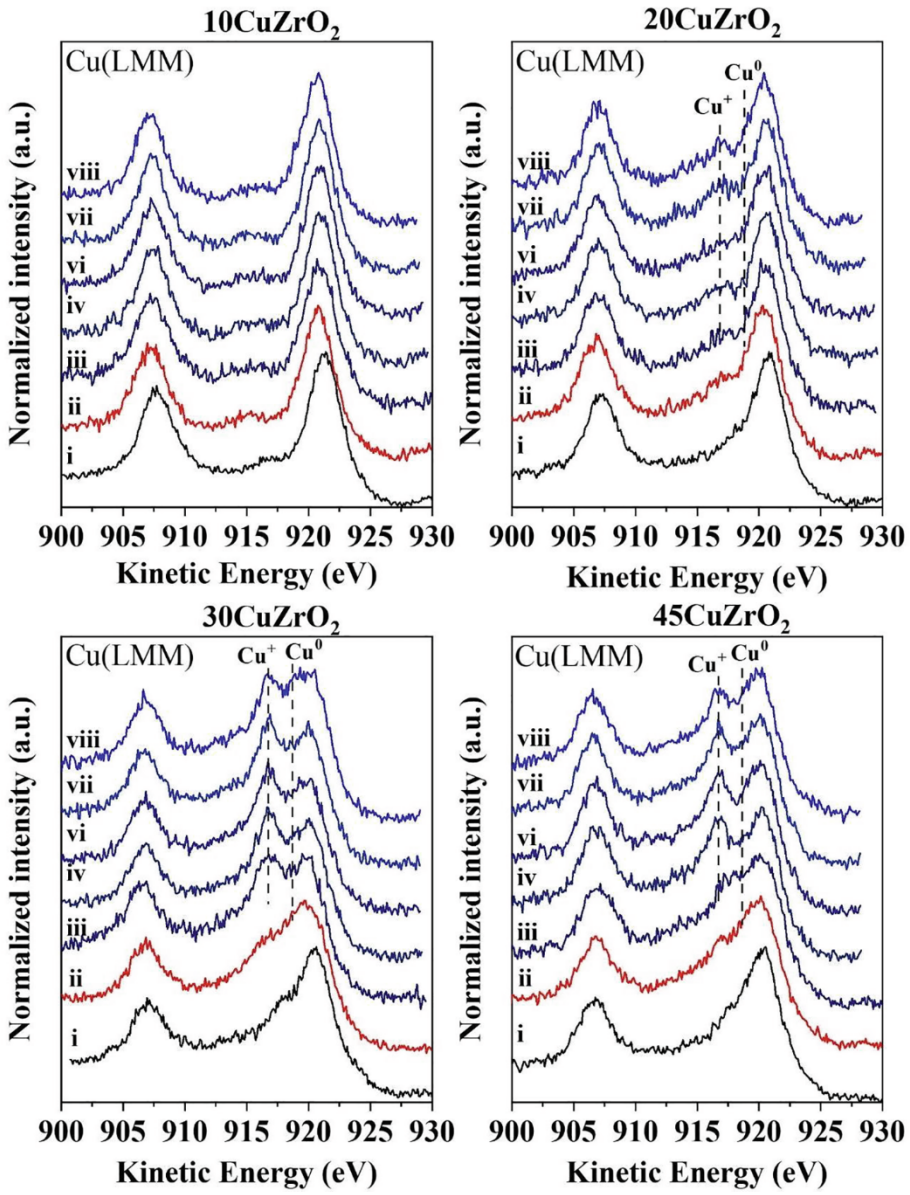

Fig. 8. AP-XPS spectra of $CuZrO_2$ catalysts in the Cu LMM Auger region. *In situ* spectra for: i) fresh, ii) reduction condition at 300 °C, (iii) 25 °C: at reaction condition, iv) 200 °C, v) 225 °C, vi) 250 °C, vii) 275 °C and viii) 300 °C. Reactant gas: CO_2/H_2 = 1:3.

3.3. *In situ characterization under reaction conditions*

The catalysts that showed high CO_2 conversion and methanol selectivity have been examined using *in situ* X-ray diffraction under activation and reaction conditions at 250 °C, as presented in Figs. 6 and 7. At room temperature, the $10CuZrO_2$ catalyst revealed only a broad peak around 32°, which is related to the amorphous phase of ZrO_2. Following an *in situ* activation process under H_2 at 250 °C, the metallic Cu face-centered cubic (fcc) phase appeared at 2θ ~ 42.2° and 49.7° (JCPDS 4-0835) [41], Fig. 6. However, the $30CuZrO_2$ catalyst, initially at room temperature, showed both a broad peak around 32° associated with amorphous ZrO_2 and peaks of the characteristic of CuO monoclinic reflections. With increasing temperature, these peaks gradually disappeared, and additional peaks related to Cu° are seen. The $30CuZrO_2$ catalyst showed the sharpest Cu diffraction peaks, indicating that the Cu crystallite size for this catalyst is larger than that of the 10CuZrO catalyst. The dissociation of CO_2 deposits atomic oxygen on copper [10]. As shown in Fig. 7, the copper remains in the crystalline metallic phase under CO_2/H_2 reaction conditions for both catalysts, suggesting that the bulk oxidation of metallic copper does not take place. Any oxygen deposited by dissociation of CO_2 is just chemisorbed and kept on the surface of the catalysts.

To ascertain the oxidation state of the catalyst surface and support the analysis of the catalytic performance, *in situ* ambient-pressure X-ray Photoelectron Spectroscopy (AP-XPS) measurements have been performed under activation conditions and a CO_2/H_2 mixture at several temperatures, as presented in Figs. 8 and 9. The O 1 s spectra is presented in the Supplementary material (Fig. S4).

Fig. 8 displays the XPS spectra for the $CuZrO_2$ samples in the Cu LMM Auger region. As shown, in the sample with lower copper content, $10CuZrO_2$, no copper oxide species have been observed on the spectra during activation and reaction conditions. Nonetheless, with increasing Cu content, the presence of Cu^+ during the reaction condition was more notable (*ca.* 916–51 – 916.75 eV). During the hydrogenation of CO_2, a fraction of the Cu^0 on the surface can be oxidized to Cu^+ by the redox mechanism on the RWGS reaction or by water, as a sub-product from methanol production or by oxygen (O*) [16,17] generated from the CO_2 dissociation [42–46]. Yet, to explore the presence of Cu^0 species, further

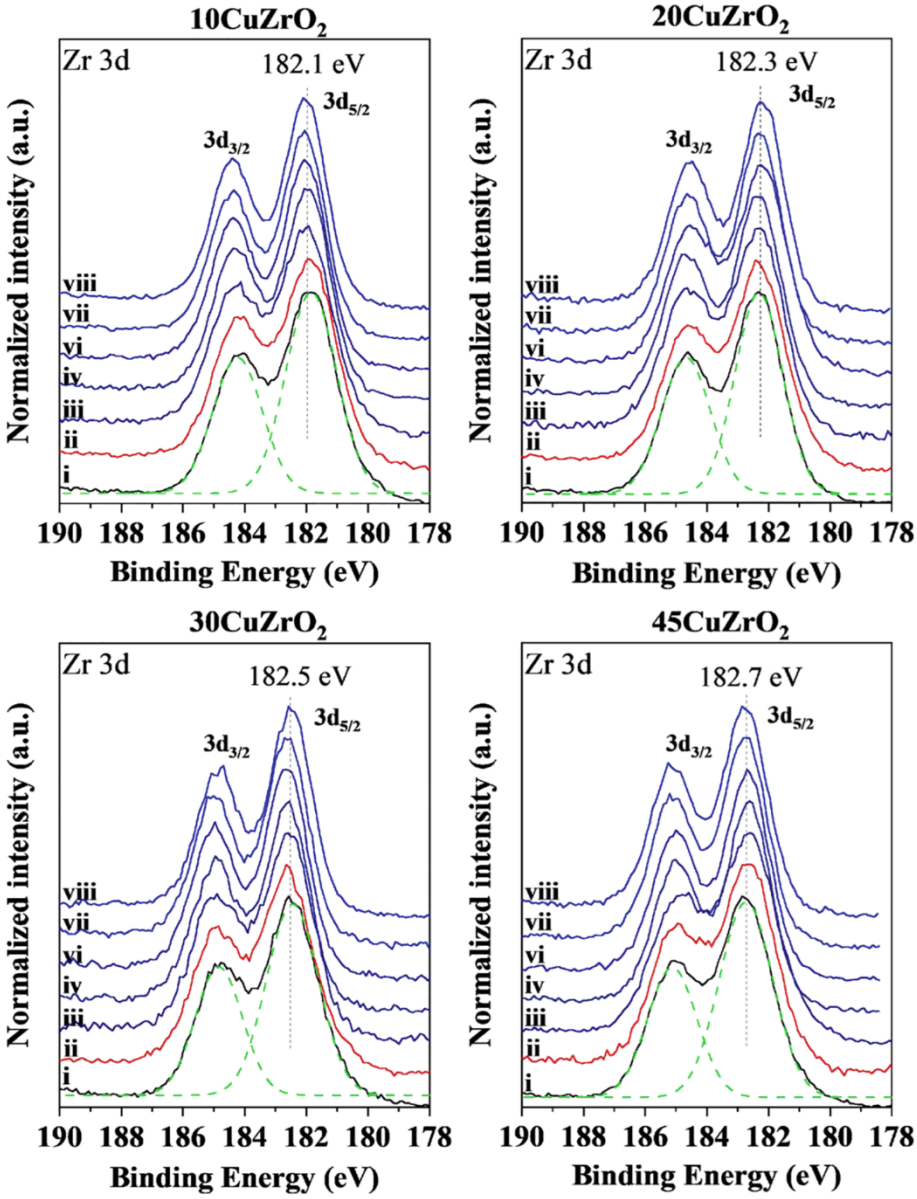

Fig. 9. AP-XPS spectra of $CuZrO_2$ catalysts in the region of Zr 3d peaks. *In situ* spectra for: i) fresh, ii) reduction condition at 300 °C, (iii) 25 °C: at reaction condition, iv) 200 °C, v) 225 °C, vi) 250 °C, vii) 275 °C and viii) 300 °C. Reactant gas: CO_2/H_2 = 1:3.

information is needed since the Zr 3p signal interferes when Mg Kα radiation is used [16,47]. With the increase in copper content, after the reduction process (ii), the spectra are broadened from 915 eV to 925 eV, suggesting the presence of Cu^0 around 918.6 eV. The increase in the Cu loading in the samples led to a shift in the binding energy of the peak, characteristic of Cu^+ species, to lower kinetic energy from 916.75 eV to 916. 51 eV, $20CuZrO_2$ and $45CuZrO_2$ catalysts.

To explore the ZrO_2 behavior under activation (H_2) and CO_2/H_2 mixture at several temperatures, Fig. 9 displays the Zr 3d spectra of samples, with spin–orbit coupling energy of 2.4 eV. As shown, the spectrum can be ascribed to the existence of zirconium species (Zr^{4+}) as the main species and all spectra were quite similar for the valence state on the surface of the fresh catalysts and during activation or reaction conditions for all materials. It showed that the chemical environment of Zr was not influenced by the activation and reaction conditions. According to the TPR analysis, the reduction of ZrO_2 species does not occur in the experimental range (from 50 to 300 °C). In addition, it was observed a positive shift of BE of Zr 3d as the copper loading increased. This shift is owing to a strong metal-support interaction (SMSI) and an indicator of charge transfer from the ZrO_2 toward the copper species.

3.4. Reaction mechanism

To gain insight into the surface species present over $10CuZrO_2$ and $30CuZrO_2$ catalysts, which exhibited the best CO_2 conversion and methanol selectivity during CO_2 hydrogenation at atmospheric pressure under different temperatures, a series of *in situ* diffuse reflectances Fourier transform infrared spectroscopy (DRIFTS) studies was performed. The vibrational peak assignment for the major surface species is listed in Table S1 in the Supporting Information. As shown in Fig. 10, at 100 °C both catalysts show bands around 2964, 2868, 1580, 1570, and 1370 wavenumbers that correspond to the assignments νas(OCO), νs (OCO), νs(CH), and δ(CH) adsorbed on the surface of the catalysts of bidentate formate (b-HCOO-Zr) [12,48–50]. Besides, three bands were observed around 2928, 2838, and 2820 cm^{-1}, with features of νas(CH_3), assigned to methoxy (CH_3O-Zr) [12,48–50]. The bands around 1310, 1570, and 1640 cm^{-1} can be assigned to νas(OCO) and νs(OCO), adsorbed on the surface of the catalysts of bidentate carbonate (b-CO_3^{2-}

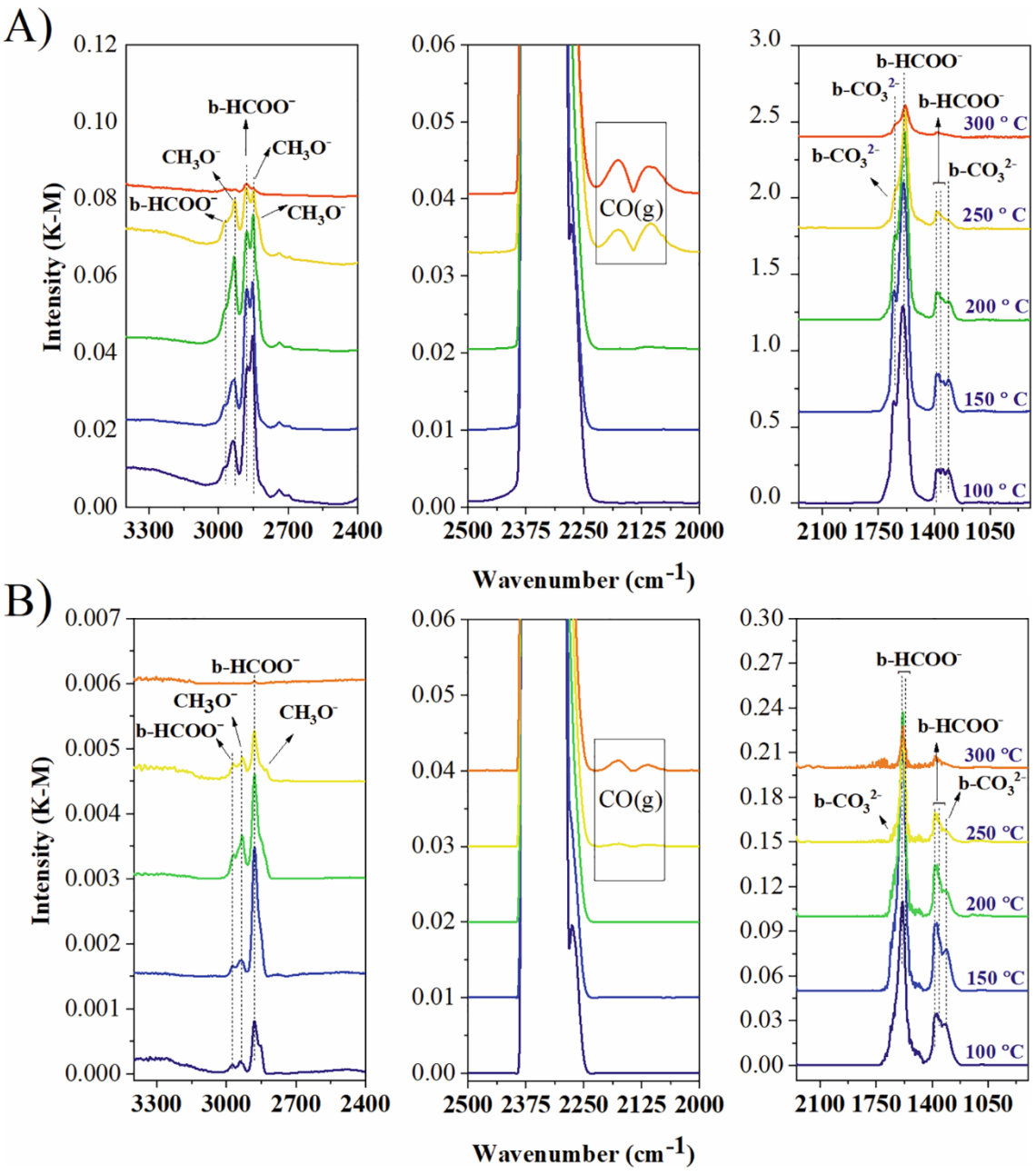

Fig. 10. *In situ* DRIFT spectra over A) $10CuZrO_2$ and B) $30CuZrO_2$ catalysts during CO_2 hydrogenation reaction (3:1 H_2:CO_2) at different temperatures.

Zr). At 1357 cm^{-1}, the presence of formate is observed on Cu (b-HCOO-Cu) [51] only for the $10CuZrO_2$ catalyst. During the reaction, the intensities of the bands of the mean intermediates, b-$HCOO^-$, CH_3O^-, and b-CO_3^{2-}, decreased with temperature increase for both catalysts. However, the intensities of the characteristic bands of bidentate formate and methoxy species are unlike among them. At 250 °C, the band characteristic of the CO gas phase was more intense for all catalysts. When the temperature rises from 250 °C to 300 °C, only the band of bidentate formate intermediate is found for $30CuZrO_2$. However, $10CuZrO_2$ catalyst presented both bidentate carbonate and bidentate formate as intermediate.

An experiment similar to subsequent switching off CO_2 from the inlet of the reactor was performed to look over the reaction pathway for methanol production from CO_2 hydrogenation on $10CuZrO_2$ and $30CuZrO_2$ catalysts. As shown in Fig. 11, IR peak intensities of surface bidentate formate and bidentate carbonate species decreased quickly after switching off the CO_2 of the reaction for both catalysts. However, the conversion of carbonates and formates into surface methoxy is much faster over the $10CuZrO_2$ catalyst, evidencing that the hydrogenation of surface carbonates/formates into methoxy is a slow step over the $30CuZrO_2$ catalyst and it might be deduced that the superior performance of $10CuZrO_2$ catalyst is because the oxygenate intermediates can be hydrogenated with a much higher rate than that on $30CuZrO_2$ catalyst under the same reaction conditions.

To gain additional insights and understand how does the $10CuZrO_2$ catalyst interacts with CO_2 and with a (CO_2 + H_2) mixture at 250 °C (Figs. 12 and 13), a new series of DRIFTS measurements were performed. Before the experiment, the material was reduced in H_2 at 250 °C for 1 h and purged by He for 5 h at the same temperature to remove the H_2 adsorbed from the Cu^0 particles. The spectra during CO_2 exposure are associated with CO_2 adsorbed species on the ZrO_2 in multiple adsorption peaks from 1700 to 1200 cm^{-1} wavenumbers, which corresponds to ν_{as}(OCO), ν_s(OCO), and δ(CH) assignments adsorbed on the surface of the catalyst. Upon exposure to the H_2 + CO_2 containing catalyst, intense

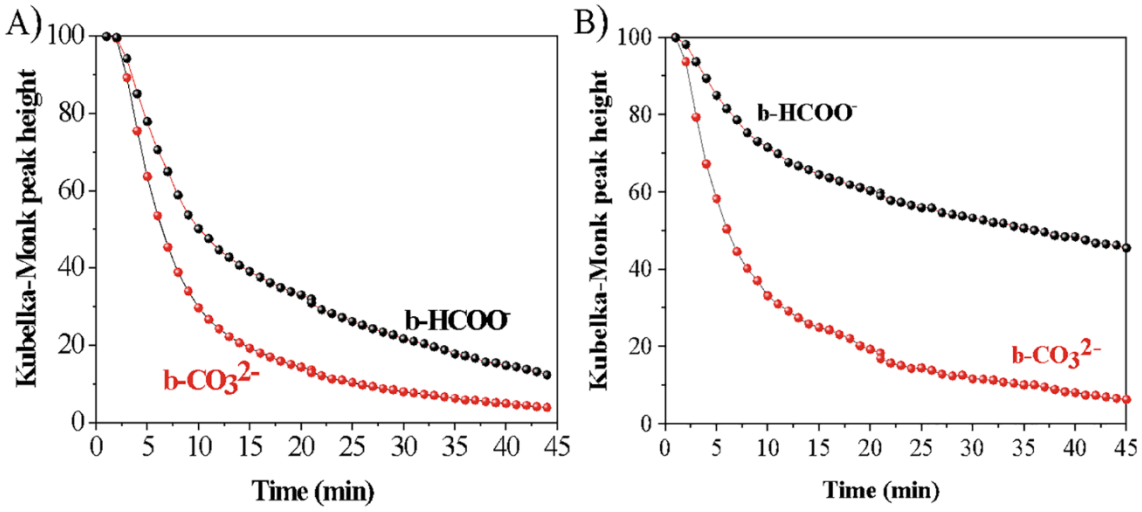

Fig. 11. IR peak intensities of surface bidentate formate and bidentate carbonate species versus time after CO_2 hydrogenation at 250 °C with switching off CO_2 over catalysts: A)10CuZrO$_2$ and B)30CuZrO$_2$, black dotted line 1581 cm^{-1} and red 1643 cm^{-1}.

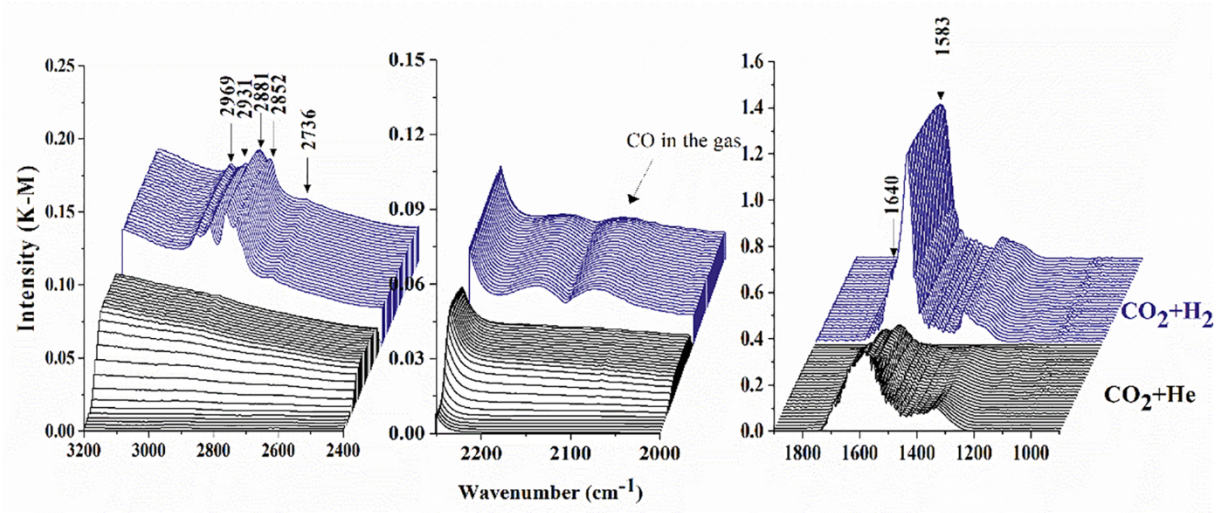

Fig. 12. *In situ* DRIFT spectra collected over 10CuZrO$_2$ reduced catalyst at 250 °C. The feed gas was switched from He to CO_2 + He, followed by a switch to CO_2 + H_2 for 30 min in each condition: H_2: 8 mL min^{-1}, He: 8 mL min^{-1}, H_2: 6 mL min^{-1} and CO_2: 2 mL min^{-1}, CO_2: 6 mL min^{-1}, and He: 2 mL min^{-1}.

broadband centered at 1583 cm^{-1} with a shoulder at 1640 cm^{-1} is observed, relating to bidentate formate and bidentate carbonate species, respectively. Also, bands have been observed at 2969 δ(CH) + ν_{as}(OCO), 2881ν(CH), 2852 cm^{-1}, and 2736 δ(CH) + ν_s(OCO), features of bidentate formate, and a band at 2931 cm^{-1} ν_{as}(CH$_3$) characteristic of methoxy species (Fig. 12).

After the knowledge of how the 10CuZrO$_2$ catalyst interacts with CO_2 and with a (CO_2 + H_2) mixture at 250 °C, a new test with subsequent switching off CO_2 was implemented on this catalyst to propose a reaction pathway. As presented in Fig. 13, some bands specific to bidentate carbonate and bidentate formate species adsorbed on the catalyst decreased quickly after switching off the CO_2 of the reaction. It shows that methanol production takes place on the surface of both Cu$^{+/0}$ and ZrO$_2$ (b-CO_3^{2-}-Zr, b-HCOO-Zr, and b-HCOO-Cu). The ZrO$_2$ surface adsorbs the CO_2 to form bidentate carbonate and formate that then undergoes progressive hydrogenation from the spillover of H atoms adsorbed on Cu$^+$/Cu^0 to the surface of ZrO$_2$ to form methoxy (CH_3O^-) and finally methanol.

3.5. Theoretical calculations of intermediates

As stated by the experimental results, the catalytic conversion of CO_2 into methanol on the surface models of perfect ZrO$_2$ and with Cu-adatom and Cu-doping was simulated. Through DFT calculations, it was found that the CO_2 adsorption may not be favored on the three models of the ZrO$_2$ catalyst surfaces (perfect, Cu-adatom, and Cu-doping), so the CO_2 molecule displays a bidentate interaction with the Zr sites according to the reaction mechanism experimentally evaluated here. In this CO_2 bidentate adsorption, the theoretical results show that the undissociated methanol intermediate is most stable during the CO_2 conversion. On specific surface models, sequent dissociation for methoxy formation could further stabilize the intermediate (Fig. 14). The desorption of the products (methanol + H_2O) is in turn energetically unfavorable. Fig. 14 shows the energies of the possible intermediates formed in the CO_2 hydrogenation into methanol on the three models of the ZrO$_2$ catalyst surface perfectly Cu-adatom and Cu-doping. The intermediates are formed over the elementary steps of CO_2 adsorption (bidentate interaction formation) and conversion into methanol (hydrogen bond formation) with possible dissociation (methoxy formation). The energy of the reactants (CO_2, H_2, and ZrO$_2$) has been used as a reference, where

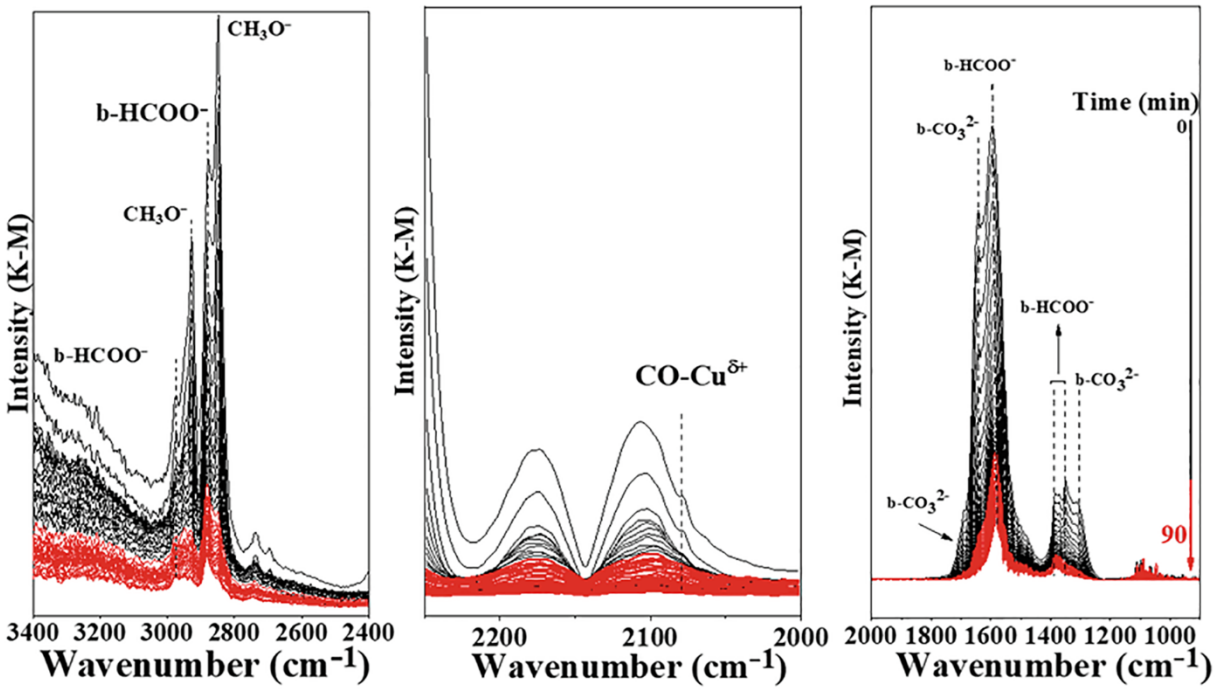

Fig. 13. *In situ* DRIFT spectra collected over $10CuZrO_2$ reduced catalyst after CO_2 hydrogenation with subsequent switching off CO_2 at 250 °C. Condition: 3:1 H_2/He during 90 min.

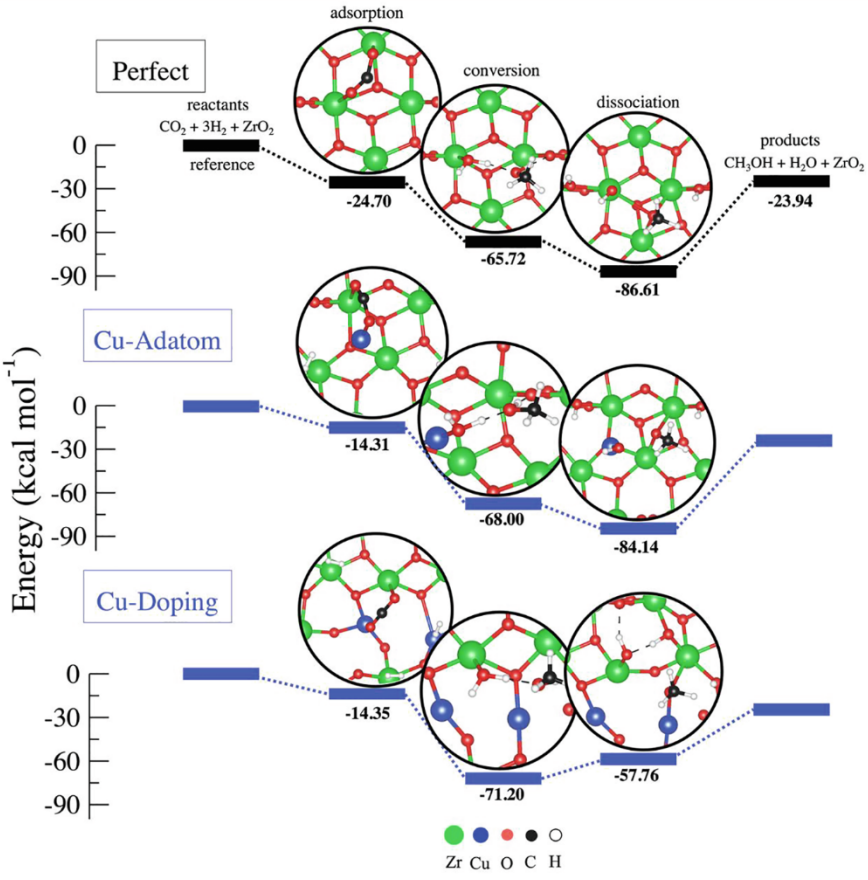

Fig. 14. Energies of the possible intermediates formed in the CO_2 hydrogenation into methanol on the three models of the ZrO_2 catalyst surfaces: perfect, Cu-adatom and Cu-doping.

ZrO_2 represents the surface model.

As stated by the energy variation, the perfect ZrO_2 surface could further favor the CO_2 adsorption compared to the surfaces with Cu. The formation energy of the intermediate adsorption on the perfect surface is approximately −10 kcal mol^{-1} most stable than on surfaces with Cu. However, the Cu-doping model was the most suitable surface for the conversion into methanol. Shorter hydrogen bond lengths of approximately 1.50 Å between the methanol and H_2O molecules and with the ZrO_2 surface are obtained for the Cu-doping surface intermediate. In addition, this Cu-doping surface does not favor the dissociation of intermediates through conversion, i.e., the conversion to methoxy from a formate intermediate [13] could be decreased. The formation energy of the dissociated conversion intermediate on the Cu-doping surface is positive (13.43 kcal mol^{-1}). For further details about the calculations of the interaction conformations and intermediate steps see the Supporting Information.

4. Discussion

Overall, the theoretical results show that the CO_2 and H_2 molecular adsorptions mainly occur on the Zr sites, despite that being the energetically less stable intermediate, and a similar statement was reported by Rui et al. [10]. Among the three surface models simulated, the CO_2 adsorption is most favorable on the perfect ZrO_2 surface. Experimentally, the lower CO_2 adsorption was indeed observed through the higher Cu concentration. From DFT calculations, Wu et al. [13] also showed that ZrO_2 islands are most active for the CO_2 activation and the CO_2 adsorption is a configuration-driven mechanism. The theoretical results also show that the conversion into methanol is most favorable with the presence of Cu in both Cu-adatom and Cu-doping surfaces, in spite, the active copper tends to be predominantly Cu^0 in Cu/ZrO_2 catalysts [52,53]. However, the ZrO_2 support alters the Cu^+/Cu^0 ratio on the catalyst surface [6].

The few amounts of Cu in the doping model could also favor increased medium basic sites in the ZrO_2 surface, as seen experimentally through the $10CuZrO_2$ catalyst with the lower concentration of Cu. Besides that, the simulated model of the Cu-doping surface may be able to limit the methoxy formation due to the decreasing electronic states of the ZrO_2 surface oxygen sites at the valence band, as seen in the projected density of states (PDOS), results in the Supporting Information. The Cu-doping model was also important to support the Zr chemical environment observed in the experimental activation and reaction conditions. Under these conditions, the temperature increase would be favorable to increase the kinetic reaction with a minor effect on the amount of Cu and methanol selectivity, as seen by the experimental results. Therefore, the intermediate steps of the catalyzed reaction of CO_2 hydrogenation into methanol may depend on the Cu incorporation in the zirconia sample, supporting the experimental results.

The catalyst with higher copper loading, $45CuZrO_2$, showed the strongest SMSI effect, as observed by XPS analysis, and lower methanol formation rate. To understand the reasons why this catalyst did not show the best methanol production is important to know the key properties to achieve a high catalytic performance to produce methanol. Then, some requirements must be fulfilled, such as a high SA_{Cu} to expose a large number of active sites, the Cu phase must be defective to achieve a high density of active sites at the surface, and strong metal–support interaction, because strong binding energy favors the pathway toward the synthesis of methanol, while weak binding energies lead to CO as a product by RWGS. Besides that, the key factor affecting the CO_2 conversion is meanly the crystallization phase of copper, which can adsorb the CO_2 differently or due to the presence of oxygen vacancy in ZrO_2 that can act as active sites for CO_2 adsorption. So, if all these issues work together the catalyst will achieve high performance for methanol synthesis [16,54].

The $30CuZrO_2$ catalyst showed the highest methanol selectivity that could be associated with a combination of a strong metal–support interaction (SMSI) with the total accessible Cu surface area (SA_{Cu}). It means that strong binding energy and high metallic surface area favor the pathway toward the synthesis of methanol. Then, only one property is not enough to achieve high catalytic performance, that is the case of $45CuZrO_2$ catalyst, that present the highest SMSI but with lowest SA_{Cu}.

Based on the combination of theory and experiments, the $10CuZrO_2$ catalyst showed the highest activity. This catalyst is the only one that has the structure of copper amorphous. The similar activity between $20CuZrO_2$, $30CuZrO_2$, and $45CuZrO_2$ catalysts could be associated with the % of medium basic sites that were very close and crucial to enhancing the methanol yield.

5. Conclusion

The $10CuZO_2$ catalyst, with the lower copper content, provided the best CO_2 conversion and methanol formation rate due to the higher copper dispersion, medium basic sites, metallic area, higher H_2 desorbed at a lower temperature, and smaller copper particle size. This catalyst displayed an amorphous crystalline structure for both CuO and ZrO_2 phases. However, the best methanol selectivity was reached at 200 °C with the $30CuZrO_2$ catalyst, which has shown a crystalline copper phase. The observed differences in the basic sites could be correlated with the crystallization phase of copper and the strong metal-support interaction with ZrO_2. The methanol formation rate was induced by both amorphous and crystalline copper phases. The Cu-doping model was a more suitable surface for the conversion of CO_2 into methanol, the same behavior of the catalyst that presented both structures in the amorphous state and without the copper segregation phase. Theoretical results also show that the CO_2 adsorption is energetically less stable main intermediate on the ZrO_2 surface with Cu. Experimentally, the lower CO_2 adsorption was indeed observed through the higher Cu concentration. The combined experiments and DFT results disclosed that the interaction between amorphous copper and zirconia could be considered a significant descriptor for the catalyst design from CO_2 to methanol through hydrogenation. Finally, the discovery of this study enhances the understanding of the effect of copper crystallization on amorphous zirconia and the rational design of catalysts for methanol production by CO_2 hydrogenation.

CRediT authorship contribution statement

Francielle C. F. Marcos: Conceptualization, Methodology, Validation, Investigation, Writing – original draft. **Raphael S. Alvim:** Validation, Investigation. **Lili Lin:** Investigation. **Luis E. Betancourt:** . **Davi D. Petrolini:** . **Sanjaya D. Senanayake:** Resources, Writing – review & editing. **Rita M. B. Alves:** Resources, Writing – review & editing. **José M Assaf:** Resources, Writing – review & editing. **Jose A. Rodriguez:** Supervision, Resources, Writing – review & editing. **Reinaldo Giudici:** Project administration, Resources, Funding acquisition, Supervision. **Elisabete M. Assaf:** Conceptualization, Supervision, Resources, Writing – review & editing, Project administration, Funding acquisition.

Declaration of Competing Interest

The authors declare that they have no known competing financial interests or personal relationships that could have appeared to influence the work reported in this paper.

Data availability

Data will be made available on request.

Acknowledgments

The authors are grateful for the financial support provided by the São Paulo Research Foundation-FAPESP (grants: 2017/08293-8 and 2018/

05799-0). The authors also gratefully acknowledge the support of the RCGI – Research Centre for Gas Innovation, hosted by the University of São Paulo (USP) and sponsored by FAPESP (2014/50279-4) and Shell Brazil. The computational time for calculations was provided by the High-Performance Computing facilities at the University of São Paulo (USP). Work done at Brookhaven National Laboratory (BNL) was supported by the U.S. Department of Energy (DOE, grant DE-SC0012704). Use of the Advanced Photon Source (beamline 17B-M) was supported by the U.S. Department of Energy under contract no. DE-AC02-06CH11357. This study was financed in part by the Personnel Coordination of Improvement of Higher Level – Brazil (CAPES) – Finance Code 001, and CNPq (grant number 310125/2021-9).

References

[1] Z. Zhang, C. Shen, K. Sun, X. Jia, J. Ye, C. Liu, Advances in studies of the structural effects of supported Ni catalysts for CO2 hydrogenation: from nanoparticle to single atom catalyst, J Mater Chem A Mater. 10 (2022) 5792–5812, https://doi.org/10.1039/d1ta09914k.

[2] K. Yang, J. Jiang, Computational design of a metal-based frustrated Lewis pair on defective UiO-66 for CO2 hydrogenation to methanol, J Mater Chem A Mater. 8 (2020) 22802–22815, https://doi.org/10.1039/d0ta07051c.

[3] X. Li, G. Liu, D. Xu, X. Hong, S.C. Edman Tsang, Confinement of subnanometric PdZn at a defect enriched ZnO/ZIF-8 interface for efficient and selective CO2 hydrogenation to methanol, J Mater Chem A Mater. 7 (2019) 23878–23885, https://doi.org/10.1039/c9ta03410b.

[4] K. Samson, M. Śliwa, R.P. Socha, K. Góra-Marek, D. Rutkowska-Zbik, J.-F. Paul, D. Mucha, M. Ruggiero-Mikołajczyk, R.M. Grabowski, J. Słoczyński, Influence of ZrO2 structure and copper electronic state on activity of Cu/ZrO2 catalysts in methanol synthesis from CO2, ACS Catal. 4 (2014) 3730–3741, https://doi.org/10.1021/cs500979c.

[5] L.C. Grabow, M. Mavrikakis, Mechanism of methanol synthesis on Cu through CO2 and CO hydrogenation, ACS Catal. 1 (2011) 365–384, https://doi.org/10.1021/cs200055d.

[6] U.J. Etim, Y. Song, Z. Zhong, Improving the Cu/ZnO-Based Catalysts for Carbon Dioxide Hydrogenation to Methanol, and the Use of Methanol As a Renewable Energy Storage Media, Front Energy Res. 8 (2020), 545431, https://doi.org/10.3389/fenrg.2020.545431.

[7] N. Razali, K. Lee, S. Bhatia, A. Mohamed, Heterogeneous catalysts for production of chemicals using carbon dioxide as raw material: A review, Renewable and Sustainable. 16 (2012) 4951–4964. http://www.sciencedirect.com/science/article/pii/S1364032112002705.

[8] S. Tada, S. Kayamori, T. Honma, H. Kamei, A. Nariyuki, K. Kon, T. Toyao, K. Shimizu, S. Satokawa, Design of Interfacial Sites between Cu and Amorphous ZrO2 Dedicated to CO2– to-Methanol Hydrogenation, ACS Catal. 8 (2018) 7809–7819, https://doi.org/10.1021/acscatal.8b01396.

[9] S. Tada, A. Katagiri, K. Kiyota, T. Honma, H. Kamei, A. Nariyuki, S. Uchida, S. Satokawa, Cu Species Incorporated into Amorphous ZrO2 with High Activity and Selectivity in CO2-to-Methanol Hydrogenation, Journal of Physical Chemistry C. 122 (2018) 5430–5442, https://doi.org/10.1021/acs.jpcc.7b11284.

[10] N. Rui, R. Shi, R.A. Gutiérrez, R. Rosales, J. Kang, M. Mahapatra, P.J. Ramírez, S. D. Senanayake, J.A. Rodriguez, CO2 Hydrogenation on ZrO2/Cu(111) Surfaces: Production of Methane and Methanol, Ind Eng Chem Res. 60 (2021) 18900–18906, https://doi.org/10.1021/acs.iecr.1c03229.

[11] A. Halder, C. Lenardi, J. Timoshenko, A. Mravak, B. Yang, L.K. Kolipaka, C. Piazzoni, S. Seifert, V. Bonačić-Koutecký, A.I. Frenkel, P. Milani, S. Vajda, CO2 Methanation on Cu-Cluster Decorated Zirconia Supports with Different Morphology: A Combined Experimental in Situ GIXANES/GISAXS, Ex Situ XPS and Theoretical DFT Study, ACS Catal. 11 (2021) 6210–6224, https://doi.org/10.1021/acscatal.0c05029.

[12] S. Kattel, B. Yan, Y. Yang, J.G. Chen, P. Liu, Optimizing Binding Energies of Key Intermediates for CO2 Hydrogenation to Methanol over Oxide-Supported Copper, J Am Chem Soc. 138 (2016) 12440–12450, https://doi.org/10.1021/jacs.6b05791.

[13] C. Wu, L. Lin, J. Liu, J. Zhang, F. Zhang, T. Zhou, N. Rui, S. Yao, Y. Deng, F. Yang, W. Xu, J. Luo, Y. Zhao, B. Yan, X.D. Wen, J.A. Rodriguez, D. Ma, Inverse ZrO2/Cu as a highly efficient methanol synthesis catalyst from CO2 hydrogenation, Nat Commun. 11 (2020) 5767, https://doi.org/10.1038/s41467-020-19634-8.

[14] Y.H. Wang, W.G. Gao, H. Wang, Y.E. Zheng, W. Na, K.Z. Li, Structure–activity relationships of Cu–ZrO2 catalysts for CO2 hydrogenation to methanol: interaction effects and reaction mechanism, RSC Adv. 7 (2017) 8709–8717, https://doi.org/10.1039/C6RA28305E.

[15] L. Lin, S. Yao, Z. Liu, F. Zhang, N. Li, D. Vovchok, A. Martínez-Arias, R. Castañeda, J. Lin, S.D. Senanayake, D. Su, D. Ma, J.A. Rodriguez, In Situ Characterization of Cu/CeO2 Nanocatalysts for CO2 Hydrogenation: Morphological Effects of Nanostructured Ceria on the Catalytic Activity, The Journal of Physical Chemistry C. 122 (2018) 12934–12943, https://doi.org/10.1021/acs.jpcc.8b03596.

[16] F.C.F. Marcos, L. Lin, L.E. Betancourt, S.D. Senanayake, J.A. Rodriguez, J.M. Assaf, R. Giudici, E.M. Assaf, Insights into the methanol synthesis mechanism via CO2 hydrogenation over Cu-ZnO-ZrO2 catalysts : Effects of surfactant/Cu-Zn-Zr molar ratio, Journal of CO2 Utilization. 41 (2020), 101215, https://doi.org/10.1016/j.jcou.2020.101215.

[17] R.M. Palomino, R. Hamlyn, Z. Liu, D.C. Grinter, I. Waluyo, J.A. Rodriguez, S. D. Senanayake, Interfaces in heterogeneous catalytic reactions: Ambient pressure XPS as a tool to unravel surface chemistry, J Electron Spectros Relat Phenomena. 221 (2017) 28–43, https://doi.org/10.1016/j.elspec.2017.04.006.

[18] F.C.F. Marcos, F.M. Cavalcanti, D.D. Petrolini, L. Lin, L.E. Betancourt, S. D. Senanayake, J.A. Rodriguez, J.M. Assaf, R. Giudici, E.M. Assaf, Effect of operating parameters on H2/CO2 conversion to methanol over Cu-Zn oxide supported on ZrO2 polymorph catalysts: Characterization and kinetics, Chemical Engineering Journal. 427 (2022), 130947, https://doi.org/10.1016/j.cej.2021.130947.

[19] K. Stangeland, H. Li, Z. Yu, Thermodynamic Analysis of Chemical and Phase Equilibria in CO2 Hydrogenation to Methanol, Dimethyl Ether, and Higher Alcohols, Ind Eng Chem Res. 57 (2018) 4081–4094, https://doi.org/10.1021/acs.iecr.7b04866.

[20] S. Scandolo, P. Giannozzi, C. Cavazzoni, S. de Gironcoli, A. Pasquarello, S. Baroni, First-principles codes for computational crystallography in the Quantum-ESPRESSO package, Z Kristallogr Cryst Mater. 220 (2005) 574–579, https://doi.org/10.1524/zkri.220.5.574.65062.

[21] P. Giannozzi, S. Baroni, N. Bonini, M. Calandra, R. Car, C. Cavazzoni, D. Ceresoli, G.L. Chiarotti, M. Cococcioni, I. Dabo, A. Dal Corso, S. de Gironcoli, S. Fabris, G. Fratesi, R. Gebauer, U. Gerstmann, C. Gougoussis, A. Kokalj, M. Lazzeri, L. Martin-Samos, N. Marzari, F. Mauri, R. Mazzarello, S. Paolini, A. Pasquarello, L. Paulatto, C. Sbraccia, S. Scandolo, G. Sclauzero, A.P. Seitsonen, A. Smogunov, P. Umari, R.M. Wentzcovitch, QUANTUM ESPRESSO: A modular and open-source software project for quantum simulations of materials, Journal of Physics Condensed Matter. 21 (39) (2009) 395502.

[22] QUANTUMESPRESSO – QUANTUMESPRESSO – (Date accessed: 2021-09-10), (n. d.).

[23] D. Chakraborty, K. Berland, T. Thonhauser, Next-Generation Nonlocal van der Waals Density Functional, J Chem Theory Comput. 16 (2020) 5893–5911, https://doi.org/10.1021/acs.jctc.0c00471.

[24] J. Qaderi, A brief review on the reaction mechanisms of CO2 hydrogenation into methanol, International Journal of Innovative Research and Scientific, Studies. 3 (2020) 53–63. https://ijirss.files.wordpress.com/2020/05/53-63.pdf.

[25] M. Sahibzada, I.S. Metcalfe, D. Chadwick, Methanol Synthesis from CO/CO2/H2 over Pd/ZnO/Al2O3: Catalyst structure dependence of methanol selectivity, Appl Catal A Gen. 118 (1998) 111–118.

[26] X. Dong, F. Li, N. Zhao, F. Xiao, J. Wang, Y. Tan, CO2 hydrogenation to methanol over Cu/ZnO/ZrO2 catalysts prepared by precipitation-reduction method, Appl Catal B. 191 (2016) 8–17, https://doi.org/10.1016/j.apcatb.2016.03.014.

[27] J. Mao, L. Qin, L. Tian, L. He, Y. Zhu, Q. Meng, G. Zhang, Hierarchical N-Doped CuO/Cu Composites Derived from Dual-Ligand Metal-Organic Frameworks as Cost-Effective Catalysts for Low-Temperature CO Oxidation, ACS Omega. 6 (2021) 29596–29608, https://doi.org/10.1021/acsomega.1c03877.

[28] G. Bonura, S. Todaro, L. Frusteri, I. Majchrzak-Kucęba, D. Wawrzyńczak, Z. Pászti, E. Tálas, A. Tompos, L. Ferenc, H. Solt, C. Cannilla, F. Frusteri, Inside the reaction mechanism of direct CO2 conversion to DME over zeolite-based hybrid catalysts, Appl Catal B. 294 (2021), https://doi.org/10.1016/j.apcatb.2021.120255.

[29] Q. Sheng, R.P. Ye, W. Gong, X. Shi, B. Xu, M. Argyle, H. Adidharma, M. Fan, Mechanism and catalytic performance for direct dimethyl ether synthesis by CO2 hydrogenation over CuZnZr/ferrierite hybrid catalyst, J Environ Sci (China). 92 (2020) 106–117, https://doi.org/10.1016/j.jes.2020.02.015.

[30] Y. Wang, S. Kattel, W. Gao, K. Li, P. Liu, J.G. Chen, H. Wang, Exploring the ternary interactions in Cu-ZnO-ZrO2 catalysts for efficient CO2 hydrogenation to methanol, Nat Commun. 10 (2019), https://doi.org/10.1038/s41467-019-09072-6.

[31] Y. Chang, C. Wang, T. Liang, C. Zhao, X. Luo, T. Guo, J. Gong, H. Wu, Sol–gel synthesis of mesoporous spherical zirconia, RSC Adv. 5 (2015) 104629–104634, https://doi.org/10.1039/C5RA23782C.

[32] W. Cao, J. Kang, G. Fan, L. Yang, F. Li, Fabrication of Porous ZrO2 Nanostructures with Controlled Crystalline Phases and Structures via a Facile and Cost-Effective Hydrothermal Approach, Ind Eng Chem Res. 54 (2015) 12795–12804, https://doi.org/10.1021/acs.iecr.5b03114.

[33] K.J.& Y.U. Nurul Jannah Abd Rahman, Anita Ramli, Tailoring the surface area and the acid – base properties of ZrO2 for biodiesel production from nannochloropsis sp, Sci Rep. 9 (2019) 16223.

[34] B. Bachiller-Baeza, I. Rodriguez-Ramos, a. Guerrero-Ruiz, Interaction of Carbon Dioxide with the Surface of Zirconia, Langmuir. 14 (1998) 3556–3564. doi: 10.1021/la970856q.

[35] F.C.F. Marcos, J.M. Assaf, R. Giudici, E.M. Assaf, Surface interaction of CO2/H2 mixture on mesoporous ZrO2: Effect of crystalline polymorph phases, Appl Surf Sci. 496 (2019), 143671, https://doi.org/10.1016/j.apsusc.2019.143671.

[36] L. Li, D. Mao, J. Yu, X. Guo, Highly selective hydrogenation of CO2 to methanol over CuO-ZnO-ZrO2 catalysts prepared by a surfactant-assisted co-precipitation method, J Power Sources. 279 (2015) 394–404, https://doi.org/10.1016/j.jpowsour.2014.12.142.

[37] T. Witoon, N. Kachaban, W. Donphai, P. Kidkhunthod, K. Faungnawakij, M. Chareonpanich, J. Limtrakul, Tuning of catalytic CO2 hydrogenation by changing composition of CuO-ZnO-ZrO2 catalysts, Energy Convers Manag. 118 (2016) 21–31, https://doi.org/10.1016/j.enconman.2016.03.075.

[38] X. Guo, D. Mao, G. Lu, S. Wang, G. Wu, The influence of la doping on the catalytic behavior of Cu/ZrO2 for methanol synthesis from CO2 hydrogenation, J Mol Catal A Chem. 345 (2011) 60–68, https://doi.org/10.1016/j.molcata.2011.05.019.

[39] M.D. Porosoff, B. Yan, J.G. Chen, Catalytic reduction of CO2 by H2 for synthesis of CO, methanol and hydrocarbons: challenges and opportunities, Energy Environ. Sci. 9 (2016) 62–73, https://doi.org/10.1039/C5EE02657A.

[40] M. Ronda-Lloret, Y. Wang, P. Oulego, G. Rothenberg, X. Tu, N.R. Shiju, CO2 Hydrogenation at Atmospheric Pressure and Low Temperature Using Plasma-Enhanced Catalysis over Supported Cobalt Oxide Catalysts, ACS Sustain Chem Eng. 8 (2020) 17397–17407, https://doi.org/10.1021/acssuschemeng.0c05565.
[41] F.C.F. Marcos, J.M. Assaf, E.M. Assaf, Catalytic hydrogenation of CO2 into methanol and dimethyl ether over Cu-X/V-Al PILC (X = Ce and Nb) catalysts, Catal Today. 289 (2017) 173–180, https://doi.org/10.1016/j.cattod.2016.08.007.
[42] F. Arena, G. Mezzatesta, G. Zafarana, G. Trunfio, F. Frusteri, L. Spadaro, How oxide carriers control the catalytic functionality of the Cu–ZnO system in the hydrogenation of CO2 to methanol, Catal Today. 210 (2013) 39–46, https://doi.org/10.1016/j.cattod.2013.02.016.
[43] X. Jiang, X. Nie, X. Guo, C. Song, J.G. Chen, Recent Advances in Carbon Dioxide Hydrogenation to Methanol via Heterogeneous Catalysis, Chem Rev. 120 (2020) 7984–8034, https://doi.org/10.1021/acs.chemrev.9b00723.
[44] E.L. Fornero, D.L. Chiavassa, A.L. Bonivardi, M.A. Baltanás, CO2 capture via catalytic hydrogenation to methanol: Thermodynamic limit vs. 'kinetic limit, Catal Today. 172 (2011) 158–165, https://doi.org/10.1016/j.cattod.2011.02.036.
[45] K. Li, J.G. Chen, CO2 Hydrogenation to Methanol over ZrO-Containing Catalysts: Insights into ZrO2 Induced Synergy, ACS Catal. 9 (2019) 7840–7861, https://doi.org/10.1021/acscatal.9b01943.
[46] S.H. Liu, H.P. Wang, H.C. Wang, Y.W. Yang, In situ EXAFS studies of copper on ZrO2 during catalytic hydrogenation of CO2, J Electron Spectros Relat Phenomena. 144–147 (2005) 373–376, https://doi.org/10.1016/j.elspec.2005.01.281.
[47] S. Velu, K. Suzuki, C.S. Gopinath, H. Yoshida, T. Hattori, XPS, XANES and EXAFS investigations of CuO/ZnO/Al2O3/ZrO2 mixed oxide catalysts, Physical Chemistry Chemical Physics. 4 (2002) 1990–1999, https://doi.org/10.1039/b109766k.
[48] J. Wang, G. Li, Z. Li, C. Tang, Z. Feng, H. An, H. Liu, T. Liu, C. Li, A highly selective and stable ZnO-ZrO2 solid solution catalyst for CO2 hydrogenation to methanol, Sci Adv. 3 (10) (2017), https://doi.org/10.1126/sciadv.1701290.
[49] A. Atakan, E. Erdtman, P. Mäkie, L. Ojamäe, M. Odén, Time evolution of the CO2 hydrogenation to fuels over Cu-Zr-SBA-15 catalysts, J Catal. 362 (2018) 55–64, https://doi.org/10.1016/j.jcat.2018.03.023.
[50] K.D. Jung, A.T. Bell, Role of Hydrogen Spillover in Methanol Synthesis over Cu/ZrO2, J Catal. 193 (2000) 207–223, https://doi.org/10.1006/jcat.2000.2881.
[51] K. Larmier, W.C. Liao, S. Tada, E. Lam, R. Verel, A. Bansode, A. Urakawa, A. Comas-Vives, C. Copéret, CO2-to-Methanol Hydrogenation on Zirconia-Supported Copper Nanoparticles: Reaction Intermediates and the Role of the Metal-Support Interface, Angewandte Chemie – International Edition. 56 (2017) 2318–2323, https://doi.org/10.1002/anie.201610166.
[52] Q. Tang, Q. Hong, Z. Liu, CO2 fixation into methanol at Cu/ZrO2 interface from first principles kinetic Monte Carlo, J Catal. 263 (2009) 114–122, https://doi.org/10.1016/j.jcat.2009.01.017.
[53] R.A. Koeppel, A. Baiker, A. Wokaun, Copper/zirconia catalysts for the synthesis of methanol from carbon dioxide, Influence of preparation variables on structural and catalytic properties of catalysts, Appl Catal A Gen. 84 (1992) 77–102, https://doi.org/10.1016/0926-860X(92)80340-I.
[54] S. Zander, E.L. Kunkes, M.E. Schuster, J. Schumann, G. Weinberg, D. Teschner, N. Jacobsen, R. Schlögl, M. Behrens, The role of the oxide component in the development of copper composite catalysts for methanol synthesis, Angewandte Chemie – International Edition. 52 (2013) 6536–6540, https://doi.org/10.1002/anie.201301419.